IR signature management for the modern navy

David A. Vaitekunas[a,1], Yoonsik Kim[b,2]
[a]W.R. Davis Engineering Limited, 1260 Old Innes Road, Ottawa, Ontario, Canada K1B 3V3
[b] Korea Institute of Ocean Science and Technology, Daejeon, Republic of Korea

Proc. SPIE 8706, Infrared Imaging Systems: Design, Analysis, Modeling, and Testing XXIV, 87060U (June 5, 2013); doi:10.1117/12.2016499

ABSTRACT

A methodology for analysing the infrared (IR) signature and susceptibility of naval platforms using ShipIR/NTCS was presented by Vaitekunas (2010). This paper provides three key improvements: use of a larger climatic data set (N=100), a new target sub-image algorithm eliminating false detections from pixel-aliasing at the horizon, and a new seeker model interfacing with a line-by-line background clutter model. Existing commercial stealth technologies (exhaust stack suppression, low solar absorptive paints, extended hull film-cooling) are re-analysed using the new models and methods to produce a more rigorous and comprehensive analysis of their effectiveness based on the statistics of reduction in IR susceptibility. These methods and results combined with the cost of each stealth option should allow platform managers to select an appropriate level of infrared suppression and establish the design criteria for a new ship.

Keywords: infrared signature, infrared detection, ship model, numerical simulation, infrared stealth, suppression, platform requirements

1. INTRODUCTION

ShipIR/NTCS is a comprehensive software engineering tool for predicting the thermal infrared (IR) signature and IR susceptibility of naval warships. The ShipIR component consists of several sub-models, including the MODTRAN5 infrared sky radiance and atmosphere propagation model, and a proprietary sea reflectance model combining the methods of Mermelstein (1994) with the results from Shaw and Churnside (1997) and Ross and Dion (2007). The platform model is created from a 3D surface geometry which forms the basis of both a radiative heat transfer and in-band surface radiance model comprised of multi-bounce diffuse and specular reflections. An exhaust plume trajectory and IR emission model predicts the infrared signature of diesel engine and gas turbine exhaust systems. Internal heat sources are modelled via user-defined thermal boundary conditions, simulating a complex thermal network of specified temperatures (controlled spaces), forced and natural convection conduits, heat-flux, and heat conduction. Validation of the ShipIR model has been the topic of numerous research papers (Vaitekunas and Fraedrich 1999, Fraedrich et al. 2003, Vaitekunas 2005).

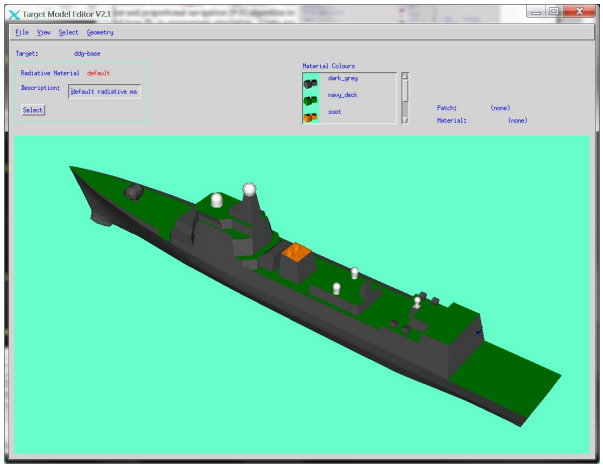

Figure 1: ShipIR model of an unclassified destroyer.

Vaitekunas (2010) described how the basic image and polar signature analysis tools of ShipIR were supplemented with an imaging seeker and proportional navigation (P-N) algorithm in NTCS to perform closed-loop fly-in engagement simulations. Users can input their own seeker models (wave-band,

[1] dvaitekunas@davis-eng.com; http://www.davis-eng.com; phone: +1 613 748 5500; fax: +1 613 748 3972

[2] yoonsik@kiost.ac; http://www.kiost.ac; phone: +82 42 866 3454; fax: +82 42 866 3449

field-of-view, array size) and detection criteria (noise-equivalent temperature difference, signal-to-noise ratio, no. of pixels, no. of frames) to analyse the polar detection range of their platform in different operating scenarios. The unclassified DDG model shown in Figure 1 was used by Vaitekunas (2010) to demonstrate NTCS methods and predict infrared detection to show the benefits of infrared stealth technology. The same model is used again to demonstrate the improvements made in the ShipIR/NTCS software and the methods used to define the operating scenarios. The new analysis considers 100 different operating environments (air and sea temperature, humidity, wind speed and direction), 2 ship speeds (18 and 29 kts), 2 diurnal conditions (day, night), 2 sensor bands (3-5µm, 8-12µm), and 2 sensor altitudes (10m, 300m). Table 1 shows the propulsion and hotel power configurations of the DDG model as a function of ship speed (for ISO conditions).

Table 1: propulsion and hotel power configurations.

Modes	2 x MTU 20V956 TB92	2 x DN80 (Ukraine)	4 x MTU 16V396	Speed (kts)
cr	12.4 MW		2.5 MW	18
fp		43.4 MW	2.5 MW	29

To demonstrate the benefits of infrared stealth design, 3 versions of the DDG model were created: a baseline version with no stealth technology (dark grey paint, no exhaust suppression), a minimum level of infrared signature suppression or IRSS (low solar absorptive or LSA paint, passive exhaust suppression), and a medium level of IRSS (passive exhaust suppression, extended hull film cooling or HFC). More advanced levels of IRSS exist but will be the topic of another paper.

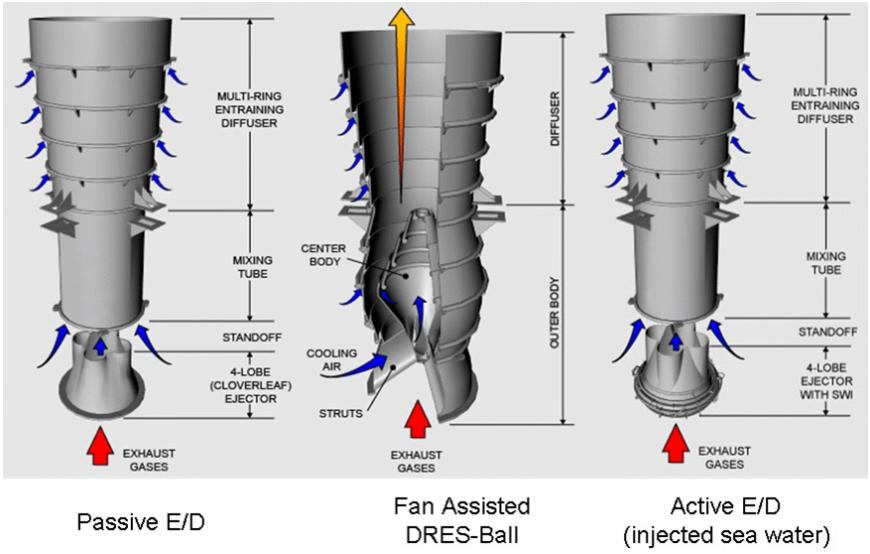

Figure 2: stack infrared suppression systems.

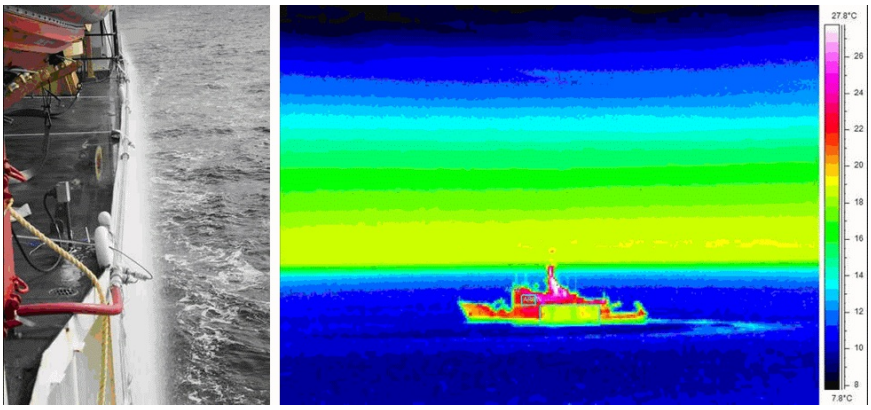

Figure 3: photograph and infrared image of an AHC system in use on the CFAV Quest.

Other than reducing the hull signature with low solar absorptive coatings or LSA paints, three common stack suppression systems in service are shown in Figure 2. The passive Eductor/Diffuser (E/D) system was selected for this study. It maintains an average metal temperature on the multi-ring diffuser to within 25°C of ambient air temperature, and dilutes both the exhaust temperature and combustion products (CO_2, H_2O, CO) by around 50%. More information on these IRSS devices can be found in Vaitekunas (2010). Research and development has also progressed on more active hull cooling measures. Figure 3 shows a visual and infrared image taken from the Onboard Signature Management (OSM) system on the Canadian Forces Auxiliary Vessel (CFAV) Quest, an unclassified Canadian Defence research vessel operated out of Halifax by the Canadian Navy and Defence Research Development Canada (Atlantic). The system uses temperature sensors installed on the inner sides of the hull, and shipboard climatic data sensors, to monitor and control the hull skin signature. Modelling the dynamics and performance of the AHC system is still beyond the current capabilities of ShipIR/NTCS. This study will focus on the ideal steady-state operation of an extended water-spray system used to achieve an equilibrium surface temperature close to sea temperature. The objective is to demonstrate its effectiveness

under a wide range of operating environments, where the air-sea temperature difference (ASTD) can vary by as much as -15°C to +5°C.

2. ENABLING TECHNOLOGY

Key improvements were made to ShipIR / NTCS (v3.5) to enable the IR susceptibility analysis on a large number of scenarios. The first one involved the target sub-image rendering algorithm used to generate accurate ship signatures at long range (Vaitekunas and Lawrence, 1999). Figure 4 shows the image analysis output from ShipIR (v3.4) for a ship at a fixed range with a varying sensor field-of-view (FOV) from 0.3° to 14°. The average target radiance (Lavg) remains constant but the average background radiance (Lbck) and average ship contrast (Lc_avg) vary markedly with sensor FOV. These fluctuations are the result of differences in OpenGL output between the sensor view and the target sub-image, a consequence of Gouraud shading and pixel aliasing. Since the purpose of the target sub-image is to feed the seeker model with accurate ship signatures, and the seeker model uses contrast radiance to perform its detection and tracking, the algorithm was modified to preserve the ship contrast instead of the ship radiance, as illustrated in Figure 5. The solution involved rendering a background-only image in both the sensor view and target sub-image, the rendering of a target-only sub-image (i.e., black background), and the processing of all 3 images to generate the sensor view with the correct ship contrast. The only caveat is that any future efforts to validate the absolute radiance of the ship will need to produce the scene image without any sub-image rendering (i.e., near full FOV image of the ship).

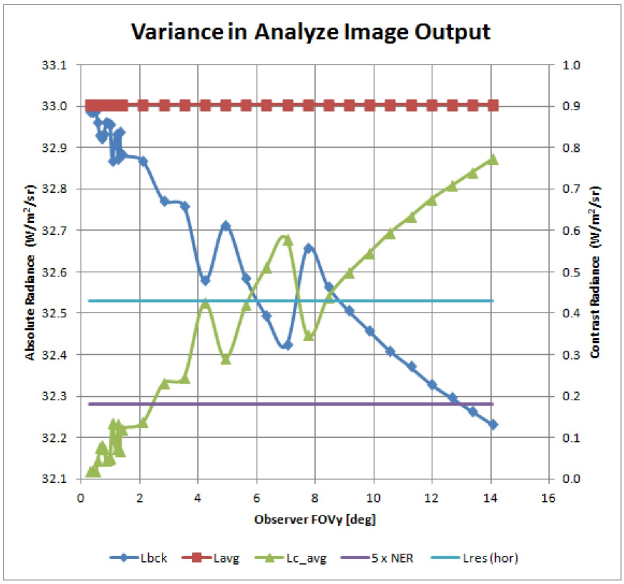

Figure 4: aliasing the background in ShipIR (v3.4).

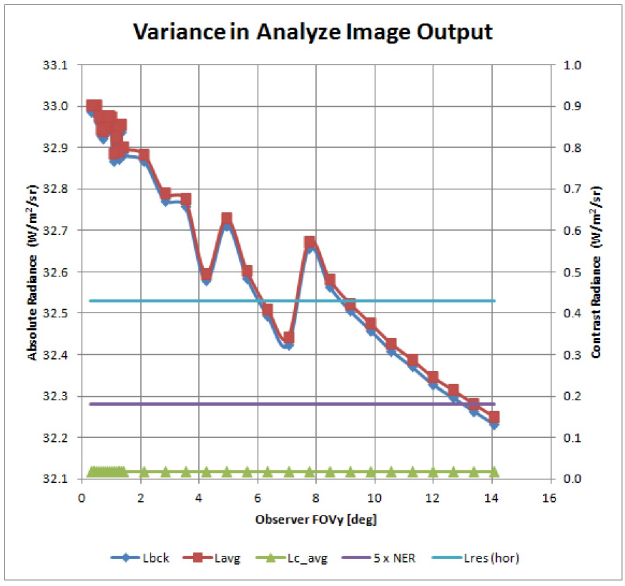

Figure 5: preserving the contrast in ShipIR (v3.5).

As described by Vaitekunas (2010), the existing seeker model in ShipIR/NTCS (v3.4) uses a line-by-line (horizontal) contrast algorithm and basic detection criteria (NETD, SNR, N_p, N_f) to declare a lock-on condition. Previous versions of the model required the user to increase the NETD for scenarios where false detections were found to occur. Some of these were likely the result of previous target sub-image defects (Figure 4), but to further eliminate any potential for false detections on the background, a new line-by-line (horizontal) background clutter model was introduced in ShipIR (v3.5). Three different sources of background clutter are used: the horizontal (azimuthal) variation in the background-only radiance image (sensor FOV),

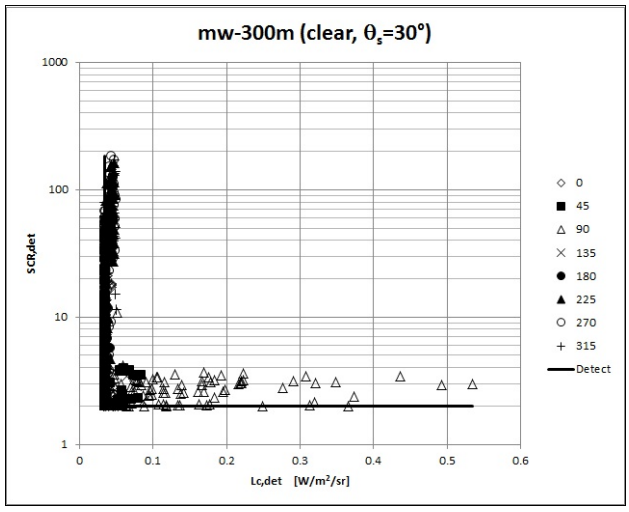

Figure 6: SCR vs Lc at detection in ShipIR (v3.5).

the special treatment of the horizon (i.e., step change in background radiance), and the processing of analytical sea clutter using methods proposed by Miller and Fraedrich (2010). The new seeker model allows the user to discriminate between noise-limited (sensor) and clutter-limited (background) infrared detection. Figure 6 shows the results from the DDG model operating under clear-sky conditions with a sun elevation of 30°, using a mid-wave (MW) 3-5μm sensor at 300m (altitude). The points clustered around the y-axis (SCR = signal-to-clutter ratio) denote noise-limited detections. Points clustered around the x-axis (Lc,det = target contrast at detection) denote clutter-limited detections. A NETD of 0.1°C and SNR of 5 translate into minimum values of 0.034 and 0.18 W/m^2/sr for Lc,det in the MW and long-wave (LW) 8-12μm sensors, respectively. The offset between the data points and either axis is due to the vertical shift in target pixels during the fly-in as they move either above or below the horizon to regions of lower clutter and higher contrast. The polar detection range analysis was also improved and optimised with the introduction of a two-phase algorithm. Phase I steps the seeker at 1 km increments towards the target to rapidly estimate the maximum detection range. Phase II performs the detailed fly-in engagement at the sampling rate specified by the user (e.g., 16 Hz). A secondary check during phase II resets the initial range (back 1 km) when detection occurs within 1 km of the initial range. Phase II continues past the first detection point (Rmax) to collect additional information about the strength of detection. New results include the minimum range for loss of detection (Rmin) and the fraction of frames between Rmax and Rmin that the platform was detectable. The new data was not used in this study, but may serve to better define platform detectability. To remove any bias associated with spurious detections, the detection range was set to Rmin in this study.

3. SCENARIO MODELLING

One of the key features in this study is the number of climatic data points (N=100) used to describe the operating environment. The history and methods behind the climatic data selection are described by Vaitekunas and Kim (2013), where approximately 10 years of hourly data from a Korean Meteorological Administration (KMA) stationary marine buoy in the Eastern Sea (37.5N, 130.0E) are used to down select 100 climatic data points. In addition to the 5 measured variables (Ta, Ts, RH, Ws, Wd), the 24-hour average wind speed was calculated for input to the Navy Maritime Aerosol Model (MODTRAN). Other considerations in the study are shown in Table 2. The two ship speeds and engine configurations are summarised in Table 1. Two CAD geometries (baseline, IRSS) and two stealth versions (LSA+IRSS, HFC+IRSS) define the 3 ship designs. The sensor characteristics and detection criteria shown in Table 3 were used for all 4 sensors.

Table 2: scenario model inputs

No. of Regions:	1	(Eastern Sea)
Environments:	100	(per region)
Diurns:	2	(day, night)
ship designs:	3	(base, LSA+IRSS, HFC+IRSS)
ship configurations:	2	(6 kts, 24 kts)
Sensors:	4	(lw, mw, 10m, 300m)
Total Scenarios:	4800	
No. of azimuths:	8	
Total no. of points:	38400	

Table 3: sensor models

Basic Characteristics	
Field of View:	12°
Resolution:	256x256
IFOV:	0.81 mrad
Detection Criteria	
NETD:	0.1°C
SNR:	5
No of pixels:	2
No of frames:	2

Both day and night conditions are simulated for each climatic data point, based on the original date. Analysis has shown no correlation between the climatic variables and the time of day. For day runs, the time was calculated such that the sun was at an elevation angle of 30°, producing a maximum contrast signature for the sea skimming (10m) sensors. For night runs, the time was calculated 12 hours from the maximum sun elevation angle to avoid any possible solar-scattering at night. To further maximize the daytime contrast signature, the ship is headed 90° CCW from the sun (i.e., starboard sun heating), and during the night, the ship was headed upwind to make the thermal signature symmetric about the bow. The variates shown in Table 2 translate into a total of 4800 scenarios, and the 8 azimuth steps specified for the polar detection range analysis translate into a total of 38,400 data points.

4. RESULTS AND ANALYSIS

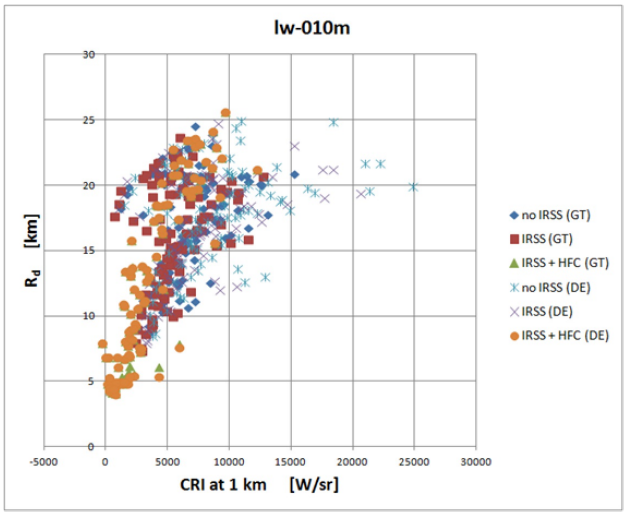

Figure 7: detection range vs CRI at 1km, 8-12μm at 10m.

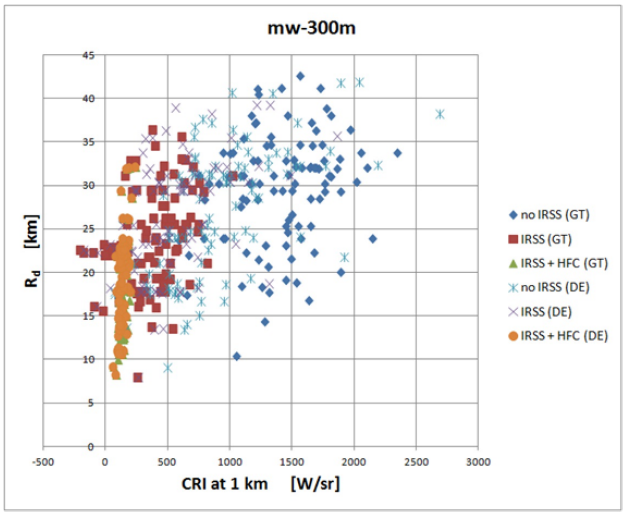

Figure 8: detection range vs CRI at 1km, 3-5μm at 300m.

Results are presented for a subset of scenarios to provide a top-level summary and justification for the methodology. Figures 7 and 8 plot the detection ranges versus total ship signature (contrast radiant intensity, CRI) for 2 of the 4 sensors. Each graph contains 600 data points corresponding to the daytime scenarios for each design configuration and a single angle of attack (launch azimuth), in this case the sun-heated side of the ship ($\Delta\phi$=+90° CW from bow). These data show how IR signature is not a simple predictor of detectability. Variations in climate cause large changes in CRI at 1km, and when combined with the atmosphere propagation (versus range) produce highly variable detection ranges. These results are significant since they provide our first evidence that detection range should be used (instead of signature) to evaluate the benefits of stealth technology. Furthermore, stealth requirements should be specified based on performance metrics of the actual IR suppression technology and not signature, since the IR signature is too variable.

4.1 Stealth Performance

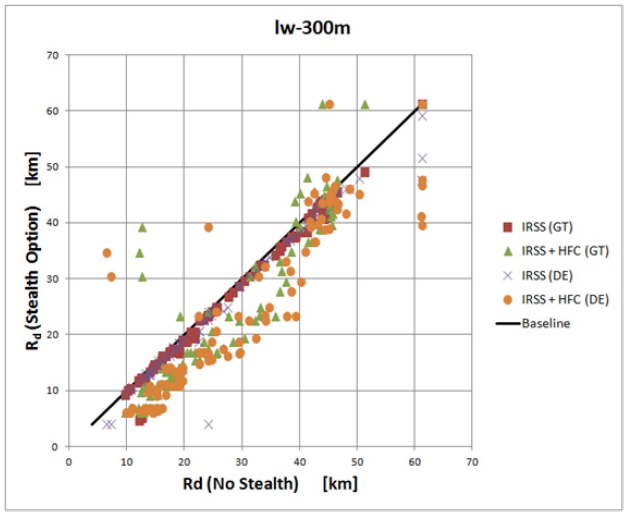

Figure 9: stealth detection vs baseline, 8-12μm at 300m.

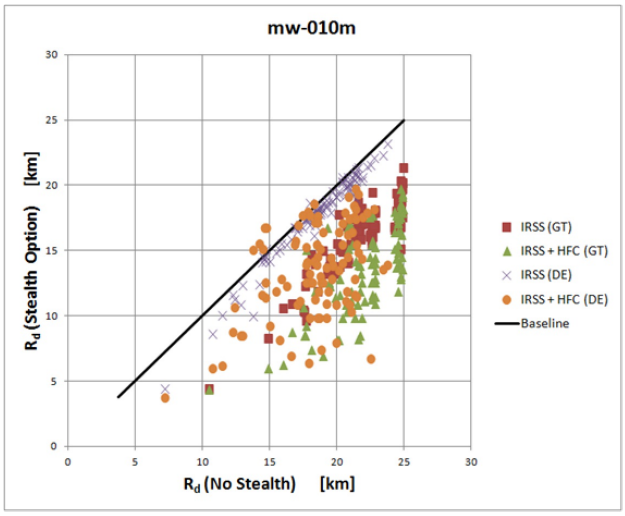

Figure 10: stealth detection vs baseline, 3-5μm at 10m.

Figures 9 and 10 show the detection range points for various stealth configurations versus that of the baseline, again for daytime scenarios along a single attack azimuth (starboard) using the two other sensors. The majority of the long-wave (8-12μm) detections are on the topside superstructure since only the combined IRSS+ HFC show any significant reduction in detection range. The mid-wave (3-5μm) data show that both engine exhaust suppression and hull wash-down are effective

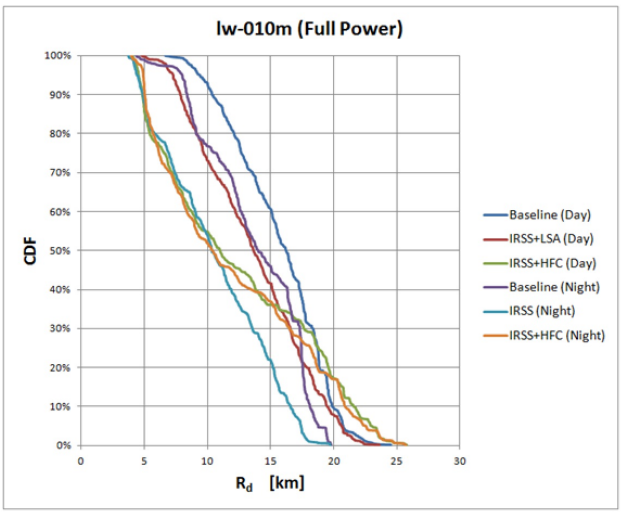

Figure 11: detection range CDF, 8-12μm at 10m.

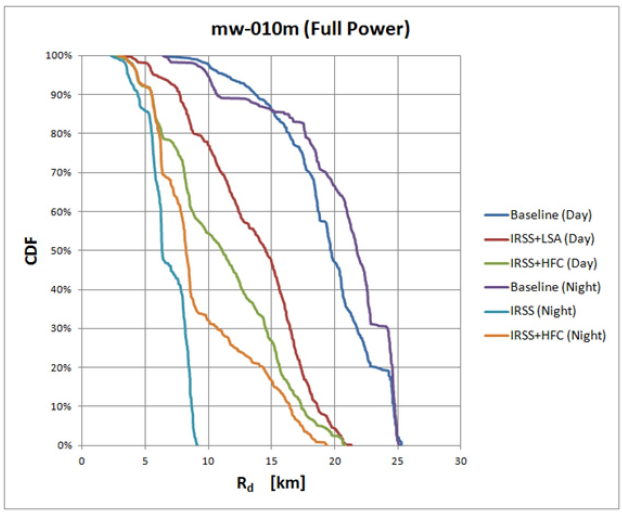

Figure 12: detection range CDF, 3-5μm at 10m.

at reducing IR susceptibility during the daytime.

To quantify the overall IR susceptibility and benefits of suppression, the data are plotted as a cumulative distribution in Figures 11 and 12. Each curve contains all the data for each design option in the full-power engine configuration, including the 8 azimuths (per sensor). In both cases, the IRSS (Night) and Baseline (Day) represent the minimum and maximum IR susceptibility, respectively. For all other configurations, the results differ between wave-band and sensor altitude. In the 3-5μm (MW), both the Baseline (Day) and Baseline (Night) are at the high-end of the detection scale, indicating the engine exhaust is a significant source of IR detection. The IRSS+LSA and IRSS+HFC are found to be incrementally effective in both wave-bands at reducing the IR susceptibility during the day. However, there is a marked degradation with use of the hull wash-down at the high end of detectability in the 8-12μm (LW) band. One of the difficulties in comparing CDF curves of detection is the missing correspondence between detection range for the same operating scenario (environment, ship speed, azimuth). To consolidate the statistics on the effectiveness of IRSS, the CDF of change in detection is plotted in Figures 13 and 14 for the following comparisons in the 8-12μm and 3-5μm at 300m:

- Effect of Daytime: Daytime: dR_d = Baseline (Day) – Baseline (Night)
- Effects of IRSS+LSA: IRSS+LSA (Day): dR_d = IRSS+LSA (Day) – Baseline (Day)
  IRSS (Night): dR_d = IRSS (Night) – Baseline (Night)
- Effects of HFC: IRSS+HFC (Day): dR_d = IRSS+HFC (Day) – IRSS+LSA (Day)
  IRSS+HFC (Night): dR_d = IRSS+HFC (Night) – IRSS (Night)

Daytime operations (dry) and hull wash-down (day and night) in the 8-12μm band show significant positive excursions in dR_d. Although large reductions (dR_d<0) do occur, they do not occupy as much of the operational space (i.e., area under the curve). Benefits are greater in the 3-5μm, where significant reductions occur for IRSS (Night), IRSS+LSA (Day), and IRSS+HFC (Day). In fact, the combined IRSS and hull wash-down during the day nearly equals the benefit of operating at night (with IRSS) in the lower 50th percentile of the CDF. These show that:

- benefits of hull wash-down at night are modest and only occur in 20% of the scenarios,
- use of hull wash-down during the day can increase IR susceptibility in 30-40% of the scenarios, indicating some decisionary logic is needed to operate the system.

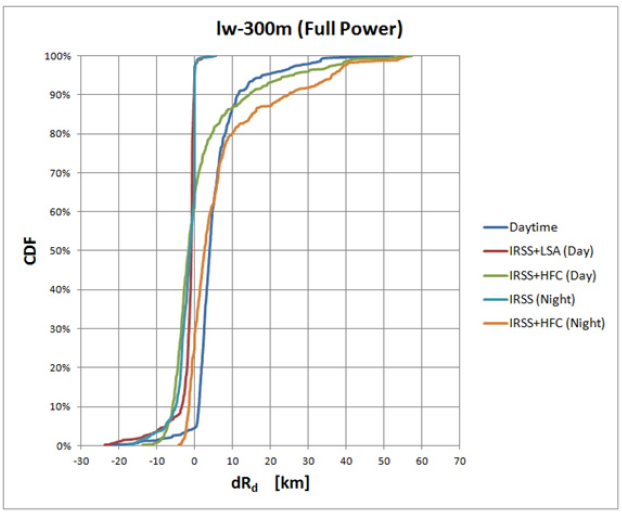

Figure 13: change in detection, 8-12μm at 300m.

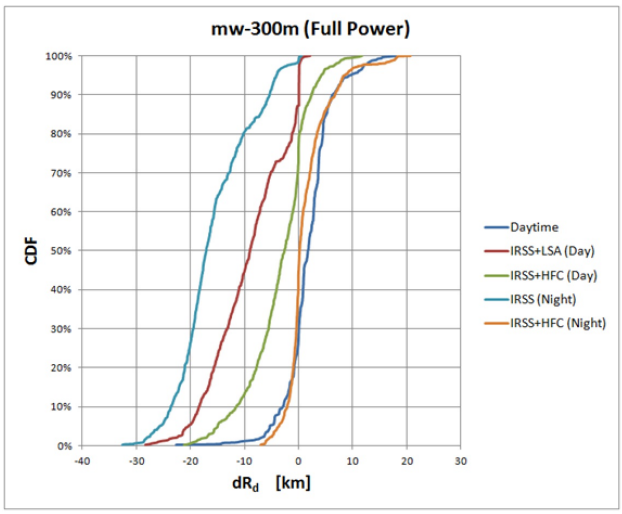

Figure 14: change in detection, 3-5μm at 300m.

4.2 Other Effects

The previous results not only demonstrated the complexity of the analysis (defining IR scenarios and predicting IR susceptibility) but also the complexity of deciding on a design approach (IR signature management). Another concern with using hull wash-down is the balancing of conflicts between the outcomes of multiple sensors operating at different wavelengths and altitudes. Because hull cooling takes time to reach thermal equilibrium (large thermal capacitance, large time constants), the system needs to be activated well in advance of a missile engagement (heightened mode), and can not be altered during the 2-3 minutes typical of a missile engagement. Three options exist for controlling the hull wash-down:

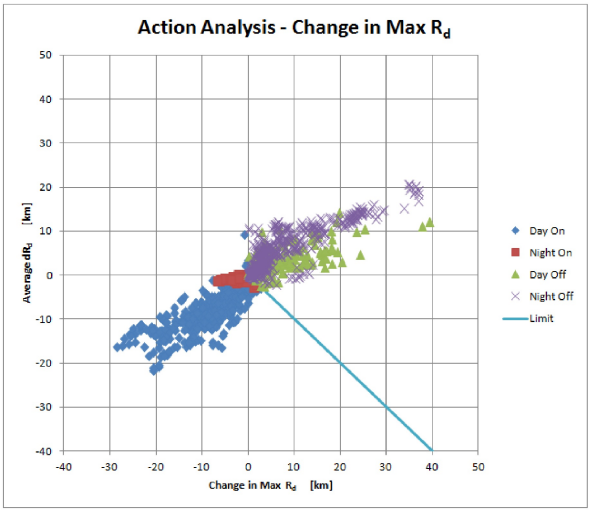

Figure 15: Average dR_d versus change in maximum R_d.

1. Simply turn on the system (full-ship) during the day in hot environments.

2. Turn on the system (full-ship) such that no increases in detection range occur (i.,e., all sensors, altitudes, and attack azimuths).

3. Turn on the system (with basic zonal / aspect control) such that the average change in detection is larger than the change in maximum detection range.

Figure 15 illustrates the outcome from the last option if we treat each azimuth point independently. On/Off zones are typically exposed to more than one attack angle, so the modes of operation can be mixed (one zone is On and one zone is Off in the same seeker view). The 3rd option is potentially more effective but would require further analysis to determine an appropriate zonal configuration and control algorithm (topic of further research).

As mentioned, one potential parameter to further optimise the hull cooling is zonal or azimuth control. Figure 16 shows the data for the change in maximum detection range versus azimuth for all sensors during the day. The HFC points show a maximum reduction on the sun-heated side of the ship (0-180°) while the maximum positive excursions (increases) occur on the shaded side of the ship (180-360°). Another key parameter in determining the effectiveness of hull film cooling is the air-sea temperature difference (ASTD). Figures 17 and 18 show the change in maximum detection range with ASTD for all the sensors, day and night, respectively. These results indicate that hull film cooling should be turned off during the

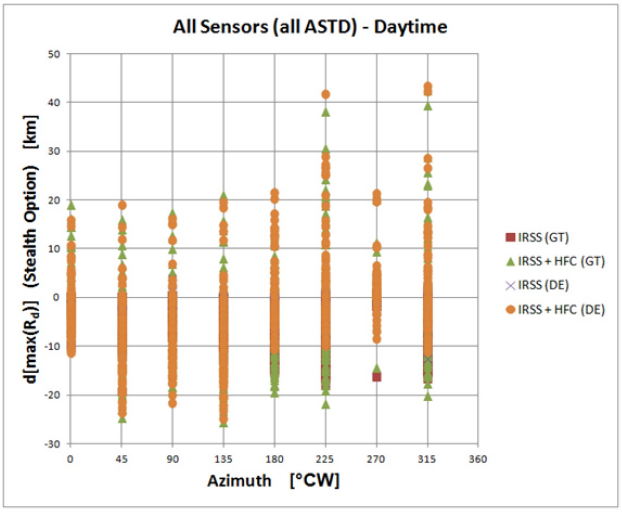

Figure 16: maximum change in R_d versus attack azimuth.

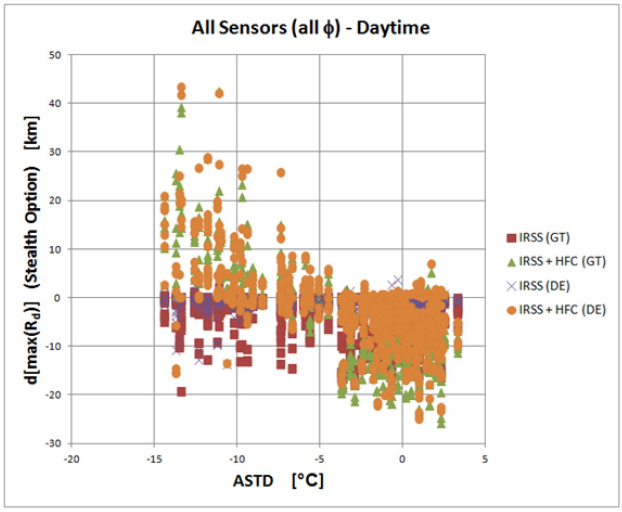

Figure 17: maximum change in R_d versus ASTD (day).

day or night when values of ASTD exceed ±5°C. The maximum reductions observed around an ASTD of 0°C makes the air temperature an obvious default set-point for the active hull cooling (AHC) system. The large scatter in the results at the same ASTD implies that other variables affect its performance.

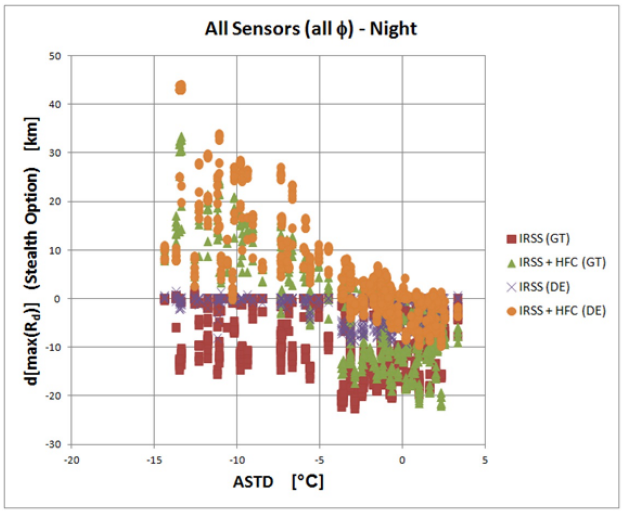

Figure 18: maximum change in R_d versus ASTD (night).

5. SUMMARY AND CONCLUSION

The percent change in detection for all the scenarios analysed are summarized in Table 4. The average or expected value, E(x), and the 5th, 50th, and 95th percentiles are listed for daytime operations and two increments in the stealth design. A few key observations are:

- Daytime operations and arbitray use of hull wash-down at night significantly increases IR susceptibility (shown in **red**).
- Exhaust IRSS shows the largest reduction in IR susceptibility at night in the mid-wave (**green**), and to a lesser extent during the day (**purple**).
- Benefits of exhaust IRSS are improved during daytime operations with an extended hull wash-down system (**bold**).
- Reductions in IR susceptibility are consistently higher in the mid-wave and GT engine configuration, thus demonstrating the importance of exhaust metal and plume suppression in reducing the IR susceptibility of the ship.

- Variations between the different sensors, altitudes, and engine configurations shows how dependent the infrared detection is on the type of signature (spectral emission) and its distribution on the ship.

This paper demonstrates recent improvements to the ShipIR/NTCS software and methods used to model and analyse IR susceptibility of naval platforms. These methods and results combined with the cost of each stealth option should allow platform managers to select an appropriate level of infrared suppression and establish the design criteria for a new ship.

Table 4: Summary of results for all options and sensors.

Analysis			% Change in Detection Range, dR_d							
Effect	Option	Sensor	Cruise Power (18 kts)				Full Power (29 kts)			
			5%	50%	95%	E(x)	5%	50%	95%	E(x)
Day vs Night	None	lw-010m	-1%	38%	144%	**36%**	0%	12%	53%	**13%**
		mw-010m	-14%	11%	286%	**17%**	-25%	0%	26%	-5%
		lw-300m	-2%	48%	426%	**51%**	1%	25%	208%	**30%**
		mw-300m	-10%	36%	666%	**58%**	-16%	7%	95%	8%
IRSS+LSA vs Baseline	Day	lw-010m	-10%	-5%	-2%	-6%	-28%	-7%	-3%	-13%
		mw-010m	-45%	-5%	4%	**-13%**	-52%	-30%	0%	**-30%**
		lw-300m	-7%	-4%	0%	-5%	-17%	-4%	-1%	-8%
		mw-300m	-24%	-12%	2%	**-14%**	-52%	-34%	0%	**-35%**
	Night	lw-010m	-11%	0%	25%	-1%	-31%	-24%	0%	-23%
		mw-010m	-79%	-72%	1%	**-71%**	-69%	-67%	-60%	**-67%**
		lw-300m	-5%	0%	4%	-2%	-21%	-8%	0%	-11%
		mw-300m	-71%	-54%	5%	**-50%**	-77%	-65%	-42%	**-66%**
IRSS+HFC vs IRSS+LSA	Day	lw-010m	-46%	-17%	63%	**-15%**	-38%	-11%	70%	**-9%**
		mw-010m	-64%	-17%	142%	**-23%**	-49%	-12%	76%	**-17%**
		lw-300m	-20%	-12%	218%	0%	-16%	-9%	294%	7%
		mw-300m	-48%	-33%	83%	**-31%**	-41%	-19%	79%	**-21%**
	Night	lw-010m	-46%	7%	154%	7%	-39%	12%	192%	**14%**
		mw-010m	-18%	37%	481%	**103%**	-4%	4%	281%	**41%**
		lw-300m	-5%	23%	671%	**44%**	-6%	20%	665%	**42%**
		mw-300m	-28%	25%	353%	**33%**	-25%	3%	176%	**17%**

6. REFERENCES

1. Cox, C. and Munk, W., "Measurement of the Roughness of the Sea Surface from Photographs of the Sun's Glitter," *J. Opt. Society Am.* 44, 838-850 (1954).

2. Fraedrich, D., S., Stark, E., Heen, L.T., and Miller, C., "ShipIR model validation using NATO SIMVEX experiment results," *Proc. SPIE* 5075, Targets and Backgrounds IX: Characterization and Representation, 49-59 (2003).

3. Mermelstein, M., D., Shettle, E., P., Takken, E., H. and Priest, R., G., "Infrared radiance and solar glint at the ocean-sky horizon," *Appl. Opt.* 33 (25), 6022-6034 (1994).

4. Miller, C., D., and Fraedrich, D., S., "Validation and Improvement of the ShipIR/NTCS Maritime Background Model," *6th International Workshop for IR Target and Background Modelling and Simulation*, 21–24 June,. Ettlingen, Germany (2010).

5. Ross, V. and Dion, D., "Sea surface slope statistics derived from Sun glint radiance measurements and their apparent dependence on sensor elevation", J. Geophys. Res., 112, C09015, doi:10.1029/2007JC004137 (2007).

6. Shaw, J.A. and Churnsize, J.H., "Scanning-laser glint measurements of sea-surface slope statistics". *Appl. Opt.* 36 (18):4202-4213 (1997).

7. Vaitekunas, D., A. and Fraedrich, D., S., "Validation of the NATO-standard ship signature model (SHIPIR)," *Proc. SPIE* 3699, Targets and Backgrounds: Characterization and Representation V, 103-113 (1999).

8. Vaitekunas, D., A. and Lawrence, O., E., "Infrared scene capabilities of SHIPIR," *Proc. SPIE 3699*, Targets and Backgrounds: Characterization and Representation V, 92 (July 14, 1999); doi:10.1117/12.352937.

9. Vaitekunas, D., A., "Technical Manual For ShipIR/NTCS (v2.9), Davis Document No. A912-002, Rev 0," (2002).

10. Vaitekunas, D., A, "Infrared Signature Instrumentation, Measurement, and Modelling of CFAV Quest for Trial Q276. Davis Document No. A320-001, Rev 0 (performed under PWGSC Contract No. W7707-3-2128)", 2004.

11. Vaitekunas, D., A., "Validation of ShipIR (v3.2): methods and results," 1st International Workshop for IR Target and Background Modelling 27–30 June Ettlingen Germany (2005).

12. Vaitekunas, D., A. "IR susceptibility of naval ships using ShipIR/NTCS," *Proc. SPIE* 7662, Infrared Imaging Systems: Design, Analysis, Modeling, and Testing XXI, 76620V (April 22, 2010); doi:10.1117/12.852131.

13. Vaitekunas, D., A., and Kim, Y., "Climatic data analysis for input to ShipIR," Proc. SPIE 8706, Infrared Imaging Systems: Design, Analysis, Modeling, and Testing XXIV, (2013).